

This is the **accepted version** of the journal article:

López-Laguna, Hèctor; Rueda, Ariana; Martínez-Torró, Carlos; [et al.]. «Biofabrication of Self-Assembling Covalent Protein Nanoparticles through Histidine-Templated Cysteine Coupling». ACS sustainable chemistry & engineering, Vol. 11, Num. 10 (January 2023), p. 4133-4144. DOI 10.1021/acssuschemeng.2c06635

This version is available at <https://ddd.uab.cat/record/284596>

under the terms of the  **CC BY** COPYRIGHT license

Biofabrication of Self-Assembling Covalent Protein Nanoparticles through Histidine-Templated Cysteine Coupling

Hèctor López-Laguna^{a,b,c,‡}, *Ariana Rueda*^{d,e,‡}, *Carlos Martínez-Torró*^a, *Lucía Sánchez-Alba*^{a,f}, *José Vicente Carratalá*^{a,b}, *Jan Atienza-Garriga*^{a,b,c}, *Eloi Parladé*^{a,b,c}, *Julieta M. Sánchez*^{a,b,c,g}, *Naroa Serna*^{a,†}, *Eric Voltà-Durán*^{a,b,c}, *Neus Ferrer-Miralles*^{a,b,c}, *David Reverter*^{a,f}, *Ramon Mangues*^{c,d,e}, *Antonio Villaverde*^{a,b,c*}, *Esther Vázquez*^{a,b,c*}, *Ugutzu Unzueta*^{b,c,d,e*}

^a Institut de Biotecnologia i de Biomedicina, Universitat Autònoma de Barcelona, 08193 Bellaterra, Spain.

^b Departament de Genètica i de Microbiologia, Universitat Autònoma de Barcelona, 08193 Bellaterra, Spain.

^c CIBER de Bioingeniería, Biomateriales y Nanomedicina, Instituto de Salud Carlos III, 28029 Madrid, Spain.

^d Biomedical Research Institute Sant Pau (IIB Sant Pau), 08041 Barcelona, Spain.

^e Josep Carreras Leukaemia Research Institute (IJC Campus Sant Pau), 08041 Barcelona, Spain.

^f Departament de Bioquímica i Biologia Molecular, Universitat Autònoma de Barcelona, 08193 Bellaterra, Spain.

^g Instituto de Investigaciones Biológicas y Tecnológicas (IIBYT) (CONICET-Universidad Nacional de Córdoba), ICTA, FCEFyN, UNC. Av. Velez Sarsfield 1611, X 5016GCA Córdoba, Argentina

KEYWORD

Protein nanomaterials, biofabrication, protein engineering, self-assembling, linker-free, covalent binding.

ABSTRACT

Nanoscale protein materials show increasing applications in biotechnology and biomedicine, addressing catalysis, drug delivery or tissue engineering. Although protein oligomerization is reachable through several engineering approaches, including the use of divalent cations for histidine-rich stretches, the effectiveness of cation-His bounding is influenced by protein conformation, media composition and chelating agents. Thus, looking for a powerful, green, cross linker-free and transversal oligomerization platforms we have built a histidine-templated cysteine-coupling concept. On this basis, we have engineered a Cys-containing, H6-derived His-Cys hybrid tag that enables the spontaneous and efficient self-assembling of tagged proteins into monodisperse nanoparticles, through a highly ordered covalent binding process. Although generated nanostructures are supported by disulfide bridge formation and exclusively reversed by reducing agents but not by chelating agents, the presence of Cysteine residues does not disrupt the metal-binding abilities of Histidine residues within the tag. This fact allows to combine the one-step IMAC-based protein purification and also, the Zn^{2+} -induced formation of higher-order microparticulate materials as nanoparticle-releasing protein-only depots. The dual mode of cross-molecular interactivity shown by the hybrid tag and the structural robustness and stability of the resulting nanoparticles offers wide applicability of the green biofabrication concept proposed here, for the further development of clinically usable protein materials.

INTRODUCTION:

Controlling the self-assembly of proteins allows the rational design and biofabrication of protein-only materials out of recombinant proteins, at the nano, micro and macro scales¹⁻⁹. In this sense, being proteins fundamental macromolecules in living organisms, the biocompatibility of such materials is ensured, allowing applications in distinct biotechnological and biomedical settings such as catalysis¹⁰, drug delivery¹¹ and regenerative medicine^{12,13}, for different functional, scaffolding or drug-packaging purposes¹⁴⁻¹⁶. On the other hand, tailoring the conformation and the biological activities of protein building blocks is reachable by conventional genetic engineering, thus allowing the generation of functional materials with refined and case-adapted functionalities. Several approaches promote regular contacts between monomers for the controlled generation of supramolecular structures. Among them, the fusion of natural or bio-inspired self-assembling domains¹⁷, the unbalance of surface charges to engineer electrostatic interactions¹⁸, the promotion of precise hydrophobic interactions¹⁹, the use of microtemplates for soft protein aggregation²⁰, the location of cysteine residues to establish disulfide bridges²¹, the use of internal disulfide bridges as molecular linkers²² and the addition of poly-histidine stretches for coordination with divalent cations²³ have proved to be effective. In particular, the accommodation of histidine-rich peptides, such as the largely used hexahistidine tag (H6), offers a broad set of biotechnological opportunities to H6-tagged proteins²⁴. These include the single-step protein purification from producing cell extracts or culture media (by Immobilized Metal Affinity Chromatography, IMAC)²⁵, and the potential for controlled cross-molecular interactions by the coordination with divalent cations, such as Zn^{2+} , Ca^{2+} and others²⁶. Since most of the recombinant proteins produced in research or pharma are His-tagged, cation-mediated assembly represents a simple and universal platform for the green biofabrication of protein nanoparticles and other more complex materials from

monomeric building blocks ²⁷⁻³⁰ , avoiding thus the use of more hazardous chemicals applied in other poorly green processes.

In our hands, the His/cation-mediated biofabrication of nanoscale protein materials has proved to be an extremely useful approach to generate precision nanoscale drugs, such as tumor-targeted nanoconjugates ³¹⁻³³ , cytotoxic protein-only constructs ³⁴ , multivalent nanobodies ³⁵ , theragnostic agents ³⁶ or antimicrobial nanoparticles ³⁷ . In these cases, cross-molecular interactions between H6-tagged proteins are promoted by the addition of divalent cations such as Zn²⁺ and Ca²⁺ at physiological concentrations. Even in this promising context, we wondered if a more refined assembling platform could be designed to offer a robust, cross-linker-free assembling process by conferring, to the building block protein, intrinsic reactivity. Avoiding the addition of external cations would make the biofabrication process and its scaling-up easier and still greener, while minimizing the potential toxicity of gluing ions in specific contexts. Also, the cation-mediated oligomerization is influenced by the conformational status and variability of the His-tagged protein, which cannot be controlled within the cell factory ³⁸ . While some His-tagged proteins self-assemble, supported by the cation content of the media, others need the external supply of such divalent cations or are produced as split of distinguishable conformer populations ³⁸ .

In this context, we envisaged the possibility to generate a linker-free protein-based assembling system with intrinsic reactivity, regardless of an additional source of external cations for histidines coordination. Interestingly, a hybrid, Cys-containing H6-derivative peptide (H3C) designed to promote covalent cross-interactivity confers, to tagged proteins, robust self-assembling through intersected cysteine residues into cross linker-free and structurally stable nanoparticles. Importantly, this innovative tool allows also to combine the original capabilities of His-based tags regarding His-mediated, single-step IMAC protein purification and the

fabrication of higher-order supramolecular constructs usable as bio-inspired microscale depots for sustained protein-drug delivery.

METHODS

Protein design and 3D structure prediction:

GFP-H3C, STM-H3C and TRAIL-H3C proteins were designed in house. 3D structures of their stable folded state were predicted *in silico* using the AlphaFold2³⁹ algorithm integrated in ColabFold⁴⁰ and using the default settings after introducing each primary FASTA sequence as query, respectively.

Protein production and purification:

Genes encoding for all proteins were provided by Genart (Thermo Fisher) already subcloned into a pET22b plasmid (Novagen), transformed into *E.coli* BL21 (DE3 OmpT⁻, Lon⁻; Novagen) and protein produced over night at 20 °C upon induction with 0.1 mM isopropyl- β -D-1-thiogalactopyranoside (IPTG). Pellets from recombinant protein-producing cells were then resuspended in wash buffer (20 mM Tris-HCl, 500 mM NaCl, 4% β -mercaptoethanol, pH 8) in presence of protease inhibitors (cOmplete EDTA free, Roche Diagnostics) and cells disrupted by 3 rounds of sonication (amplitude 10%, pulse on/off: 0.5, 5 min for round 1 and 2 and amplitude 15%, pulse on/off: 0.5, 5 min for round 3). Cell soluble fraction was separated by centrifugation at 15,000 g for 45 min and 4 °C and then filtered (0.22 μ m) before protein purification. Samples were kept on ice during all the process.

Recombinant proteins were purified from cell soluble fractions by Immobilized Metal Affinity Chromatography (IMAC) with a 5 mL HisTrap HP columns (Cytiva) in an Äkta pure system (Cytiva). Protein elution was achieved by a linear gradient of elution buffer (20 mM Tris-HCl, 500 mM NaCl, 500 mM Imidazole, 4% of β -mercaptoethanol, pH=8). Pure GFP-H3C protein was dialyzed against sodium bicarbonate with salt (166 mM NaCO₃H, 333mM pH 8) solution.

STM-H3C and TRAIL-H3C were dialyzed against sodium bicarbonate without salt (166 mM NaCO₃H, pH 8).

Protein purity, concentration, and integrity

Protein physicochemical analysis was performed as described elsewhere²⁷ and primary protein sequence properties (Figure 1A) extracted from ProtParam online software (Expasy)⁴¹.

Morphometric characterization of nanostructures:

Volume size distribution and zeta potential of protein samples were determined by Dynamic Light Scattering (DLS) and Electrophoretic Light Scattering (ELS) respectively at 633nm (25°C as a standard temperature) in a Zetasizer Advance Pro (Malvern Instruments). All samples were measured at least in triplicate and data expressed as mean ± standard error.

The average molar mass of GFP-H3C nanoparticles was experimentally determined by size exclusion chromatography coupled to a multi angle light scattering (SEC-MALS) and the number of monomers then extrapolated per nanoparticle. For that, 200 µg of nanoparticle sample were injected in a Superdex 200 Increase 10/300 (Cytiva) and run in a sodium bicarbonate with salt solution (166 mM NaCO₃H, 333mM NaCl, pH 8) . Eluent was monitored by in-line UV-vis detector, a Dawn Heleos MALS detector and an Optilab rEX RI detector (Wyatt Technology Corporation). All data were finally analyzed in an Astra 6.0.2.9 software (Wyatt Tehcnology Corporation).

High-resolution electron microscopy images of protein nanoparticles were obtained by transmission electron microscopy. For that, 5 µL droplets of nanoparticle samples (at 0.05 mg mL⁻¹) were placed on top of glow-discharged 200 mesh carbon-coated copper grids (Electron Microscopy Science) for 1 min. Then, excess of liquid was blotted with a Whatman filter paper, and protein negatively stained with 5 µL of 1 % uranyl acetate (Polysciences Inc.) for 1 min and blotted again. Grids were finally dried at room temperature for at least 10 min and high-resolution images acquired in a TEM Jeol 1400 (Jeol Ltd.) operating at 80 kV and equipped

with a Gatan Orius 8 9 SC200 CCD camera (Gatan Inc.). The most representative images were captured from different fields at 20,000x and 25,000x magnifications.

Morphometric characterization of microstructures:

High-resolution images of cation-induced microparticles were obtained by field emission scanning electron microscopy (FESEM). For that, 20 μL of each microparticle sample (0.3 mg mL^{-1}) were directly deposited on silicon wafers (Ted Pella Inc.) for 30 s and immediately observed without coating in a FESEM Zeiss Merlin (Zeiss) operating at 1 kV and equipped with a high resolution secondary electron detector. Wide field Optical microscopy images of protein microparticles were also obtained in a NIKON Eclipse Ts2R-FL microscope at x10 magnification.

Nanoparticles stability against chemical and thermal treatments

Volume size distribution of protein nanoparticles (2 mg mL^{-1}) was evaluated by DLS in presence of increasing concentrations of different reducing agents (TCEP, DTT, β -Mercaptoethanol), cation-arresting agents (EDTA, Imidazole), NaCl and Zinc II. Nanoparticles stability was also evaluated at increasing temperatures from 4 to 80°C , upon incubation at 4 and 37°C for 10 days and upon 5 consecutive cycles of thawing and freezing.

Nanoparticles zeta potential was evaluated at different temperatures from 4 to 70°C by ELS (80°C was not technically supported).

Cation-assisted nanoparticles re-assembling and disulfide formation:

EDTA and TCEP-disassembled GFP-H3C monomers were dialyzed against a cation-free sodium bicarbonate with salt solution ($166 \text{ mM NaCO}_3\text{H}$, 333 mM NaCl , pH 8) and against the same sodium bicarbonate with salt solution supplemented with 0.4 mM of cationic zinc (Zn^{2+}). GFP-H3C protein remained as monomers in the cations-deficient sodium bicarbonate solution while the presence of Zn^{2+} assisted nanoparticle re-assembling. Generated nanoparticles were then dialyzed against an alkaline sodium bicarbonate with salt solution ($166 \text{ mM NaCO}_3\text{H}$, 333 mM NaCl , pH 10) in order to favor cysteine thiol oxidation ($\text{pKa } 8.32$), and were then

immediately re-dialyzed against regular sodium bicarbonate salt solution (166 mM NaCO₃H, 333mM NaCl, pH 8) to restore original pH.

Protein structural analysis

Protein secondary structure was studied experimentally, using circular dichroism as described elsewhere ⁴². Protein tertiary structure was also studied experimentally by measuring the fluorescence emission of both GFP chromophore and tryptophan excited at $\lambda_{ex}=295$ nm, as described elsewhere ⁴².

Nanoparticles solubility in FDA-approved solutions

Protein solubility was assessed against different FDA-approved solutions (see table S1) by microdialysis. For that, 25 mL of each tested solution were poured in an empty plate and a MCE (mixed cellulose esters membrane) filter membrane of 0.025 μ m (VSWP02500 MF-Millipore, Merck®) gently settled on the surface. Next, five 20 μ L droplets from a 2 mg mL⁻¹ protein stock solution (total of 100 μ L per filter) were incubated for 50 min at room temperature, and plates covered to minimize evaporation. Then, the protein solution was carefully recovered and centrifuged at 15,000 g for 40 min at 4 °C to separate soluble protein from insoluble fraction. Finally, both the initial and final protein concentrations were measured at a 280 nm wavelength in a Nanodrop® TM One (Thermo Fisher) to extrapolate the percentage (%) of precipitation. A GFP-H3C protein sample was dialyzed against the same storage solution (namely 166 mM NaCO₃H + 333 mM NaCl, ph 8) and used as a solubility control (100%) .

Cell viability assay:

HeLa cells (ATCC, CCL-2) were incubated in opaque 96-well plates in MEM alpha medium (Gibco) containing 10 % of fetal bovine serum (Gibco) in humidified atmosphere and 5 % CO₂ at 37 °C. Then, cytotoxicity of GFP-H3C nanoparticles was evaluated by CellTiter-Glo® Luminescent Cell Viability Assay (Promega) in a Victor 3 luminescent plate reader (Perkin Elmer) upon incubation at 1, 2 and 4 μ M for 48h. All experiments were performed in triplicate and results expressed as percentage (%) of cell viability \pm standard error.

Statistical analysis:

Preliminary normality and lognormality tests (Anderson–Darling, D’Agostino and Pearson, Shapiro–Wilk and Kolmogorov–Smirnov) were performed to confirm a normal data distribution. Parametric data was analyzed by one or two-ways ANOVA or t-tests depending on the number of groups and conditions. Meanwhile, nonparametric data was analyzed by Kruskal–Wallis test. All measurements were performed at least in triplicate, peak values expressed as mean \pm standard error (SE), and significance was considered (*) when $p < 0.05$.

RESULTS AND DISCUSSION:

In IMAC-based protein purification, a few clustered His residues are required for an efficient binding of His-tagged proteins to the immobilized metal ^{43–45}. Since the combination of Cys and His residues promotes protein crystallization ⁴⁶, we presumed that a limited number of Cys residues intersected in the conventional H6 tag should confer His-independent oligomerization capabilities to the carrier protein, hopefully keeping its IMAC retention. In this regard, for divalent metal binding, a distribution of His residues alternated with a substituting (X) amino acid (H-X-H-X-H-X, etc) is required ⁴⁷. This is because the overall binding forces between C-terminal His residues with a divalent cation (expressed as KD; dissociation constant or as in μM) are majorly contributed by the positions i and $i+2$. On the other hand, three Cysteine residues are mechanistically identified as the minimal number envisaging the generation of oligomers beyond mere dimers, and also, as an adequate value to avoid complex multivalent network linking. Such ‘three’ value was supported by previous studies on hepatitis E virus-like particles (VLPs) ⁴⁸ and modified green fluorescent proteins (GFPs) ^{49,50}, in which their self-assembling properties were ablated when the number of Cys residues in the cross-interactive stretches were reduced below three. Therefore, by combining these concepts, a His-Cys hybrid

tag, that contains such minimum number of cysteines, was designed as HHHCHCHCH (H3C), by alternating those three cysteine residues starting from the C-terminal of the H6 tag sequence.

Then, a fusion GFP-H3C protein was genetically designed and its 3D structure and physicochemical parameters in silico predicted (Figure 1A). The recombinant protein was successfully produced and purified from *Escherichia coli* by IMAC chromatography (Figure 1B), resulting in a full-length, proteolytically stable single molecular species of 27.78 kDa (Figure 1C). This was indicative of a full N-terminal methionine processing as expected from its primary sequence (figure S1)⁵¹. The obtained protein construct showed a clear tendency to oligomerization that was initially observed through a minor occurrence of dimeric and trimeric forms (Figure 1C, right). When analyzed by DLS, GFP-H3C was observed as monodisperse nanoparticles of 10 nm, in contrast to the parental GFP-H6 that was compatible with the monomeric form of the protein (5 nm, Figure 1D). Importantly, the H3C tag allowed efficient protein purification being the clustering and distribution of His residues within the hybrid tag sufficient for a good IMAC performance (Figure 1B). Regarding protein stability, the thermal aggregation of GFP-H3C nanoparticles occurred at 70 °C, similar to that of the parental unassembled GFP-H6 (Figure 1E). Moreover, the zeta potential of GFP-H3C nanoparticles remained negative at physiological temperature (Figure 1F), what was seen as opportune envisaging the potential in vivo applications of the material, as in drug delivery. Finally, a fine proteomic analysis of GFP-H3C revealed that nanoparticles were formed by 6 monomers (Figure 1G), expectedly organized in a radial form from the C-terminal tag (Figure 1H). In this model, the GFP beta-barrels are distributed around the cluster of overhanging H3C peptides, sited in the core of the nanoparticle. A refined TEM analysis of the material (Figure 1 I) was compatible with such radial distribution, the nanoparticles showing a regular circular architecture with a less dense core, which could correspond to the region of the interacting tags (Figure 1 I, inset).

Considering the hybrid nature of the H3C tag, namely His and Cys residues both showing different cross-linking abilities, we explored which type of forces determined the assembling of GFP-H3C. As observed, nanoparticles were disassembled in a set of reducing media (Figure 2A), while imidazole or EDTA did not have any disrupting effect on the material (Figure 2B). This fact, apart from proving the reversible nature of the cross-molecular protein-protein contacts, indicated that His-mediated coordination of divalent cations (but disulfide bridges) were not supportive of the final architecture of the supramolecular complexes. Also increasing the ionic strength of the medium was not affecting the formed structures (Figure 2C), proving that electrostatic interactions were neither the main driving forces for the assembling. In this sense, although the cations from the media were not enough to support the final particle architecture, they might show, at least during the initial steps of nanoparticle assembling, an influence in monomers orientation, leading to a histidine-templated cysteine coupling concept. This is observed when cations-arrested and disulfide-reduced GFP-H3C monomers (EDTA + TCEP) remained unassembled in a divalent cation-deficient sodium bicarbonate solution (SB), but re-assembled in the presence of cationic zinc (Zn^{2+}) (Figure 2D). Then, a transient alkaline pH-favored re-oxidation of cysteines (Ox), in the cation-promoted particles, produced again supramolecular complexes that were only fully disassembled in presence of the disulfide disrupting agent TCEP, but not upon mere cation arresting with EDTA (Figure 2E).

Going further, the addition of an external supply of cations at high concentration (0.5 mM Zn^{2+}), also allowed to maintain these supramolecular complexes even in presence of the reducing agents (Figure 2F), while the addition of still higher concentrations of Zn^{2+} induced the organization of GFP-H3C as larger-scale microparticles (Figure 2G), that completely disintegrated upon the addition of EDTA. These observations further indicated that although histidine residues within the Cys-His tag were not responsible for the final nanoparticle architecture, at least at the cations concentration in the medium, they still maintained the

capacity to keep the supramolecular complexes just by cation coordination (in absence of disulfide bridges) at higher Zn^{2+} concentration, as parental H6-tag does ²³. Moreover, it also indicated that histidine residues within the hybrid tag were available for cation-mediated microparticle organization, in a fully reversible process. This observation is important as the formation of Zn-mediated microparticles results in highly interesting artificial materials ⁵², that like bacterial inclusion bodies ^{53,54}, show protein-leaking properties ^{28,52}. Then, mimicking metal-based amyloid fibers ⁵⁵⁻⁵⁸, Zn-mediated protein-only microparticles represent promising slow protein delivery systems for the *in vivo* administration of protein drugs ^{52,59}. Therefore, the His-Cys hybrid tag proposed here, not only assisted nanoparticle formation through covalent disulfide bridge formation, but also, assisted protein clustering as micro-scale granules upon the addition of cationic Zn from an external source. Both assembling mechanisms, reversible by either reducing agents or EDTA respectively, offer an unexpected versatility to the protein material resulting from H3C-tagged building blocks.

Focusing on the resulting nanoparticles as potential drug carriers or for other clinically-oriented applications, we tested the stability of the material under physiological conditions. A high stability, probably associated to a structural rearrangement of the secondary and tertiary protein structure was observed through tryptophan and chromophore fluorescence emission (Figure 3A) and through particular patterns in the dichroism profile (Figure 3B) compared to the control GFP-H6. On the other hand, nanoparticles were essentially soluble in most of the tested FDA-approved solutions (Figure 3C, table S1) and in all of them, the soluble protein fraction kept the 10 nm organization (Figure 3D). In addition, the material was stable upon incubation under different conditions including physiological temperature and thawing/freezing cycles (Figure 3E), and it was nontoxic over cultured mammalian cells when exposed at high concentrations (Figure 3F). Finally, the molecular size of monomers and oligomers were always consistent with the DLS data through the whole protein purification process from bacterial extracts, that

includes a reducing agents-mediated disassembly and further reassembly of the material through dialysis (Figure 3G).

In the context of the robustness shown by the H3C tag in promoting protein oligomerization as regular nanoparticles but also looking at its plasticity to keep the His-mediated potential for purification and formation of disintegrating microscale materials, we wanted to ensure that such performance was not linked to the particular beta-barrel structure of GFP, selected here as a model. Thus, to evaluate the transversal applicability of the proposed H3C tag in promoting nanoparticle formation from tagged monomers, two additional non-related and structurally divergent proteins, namely Stefin A (STM)⁶⁰ and the antitumoral protein TRAIL⁶¹, were engineered for H3C display at their C-terminus (Figure 4A, figure S1). As expected, both proteins were successfully produced as a proteolytically stable full-length proteins (figure S2 and S3). Then, as in GFP (27.78 KDa), STM (12.35 KDa) and TRAIL (20.88 KDa) spontaneously assembled into small oligomers of 5.89 and 8.66 nm respectively upon purification that were also not disassembled by mere cation arresting (EDTA) but by disulfide bridge disruption with TCEP (Figure 4B). Moreover, the new constructs were stable at physiological temperatures (Figure 4C) and were also able to organize into larger-scale microparticles upon addition of cationic zinc at high concentrations (Figure 4D and S4).

CONCLUSIONS

The proper combination of His and Cys residues in a C-terminal peptidic tag (HHHCHCHCH) allows to promote, by genetic fusion, the spontaneous oligomerization of tagged proteins into regular nanoparticles, irrespective of the addition of external linkers. The regularity of the resulting nanoparticles, their high stability and the fact that their formation is not restricted to a particular structure of the core protein makes the very simple strategy proposed here of universal interest for the design of green protein nanoparticles out from any potential protein

candidate, by very simple genetic engineering. While the formation of the final nanoparticles is supported by covalent disulfide bonding, the His residues within the hybrid tag still may show a certain influence in the initial orientation of the monomers, leading to a histidine-templated cysteine coupling. Moreover, His residues within the tag allow also the efficient one-step protein purification as well as the controlled formation of more complex, microscale particles upon the addition of external cationic Zn, through His coordination. The possibility to generate larger-order materials based on Zn^{2+} is interesting as they are self-disintegrating biomimetic materials highly suited for slow protein drug delivery in vivo. Under the present setting, the released materials are nanoparticles formed by covalent disulfide-bonded building blocks. Thus, the dual mechanism by which the hybrid His-Cys tag performs, offer two options for the construction of green protein biomaterials suited for clinical applications.

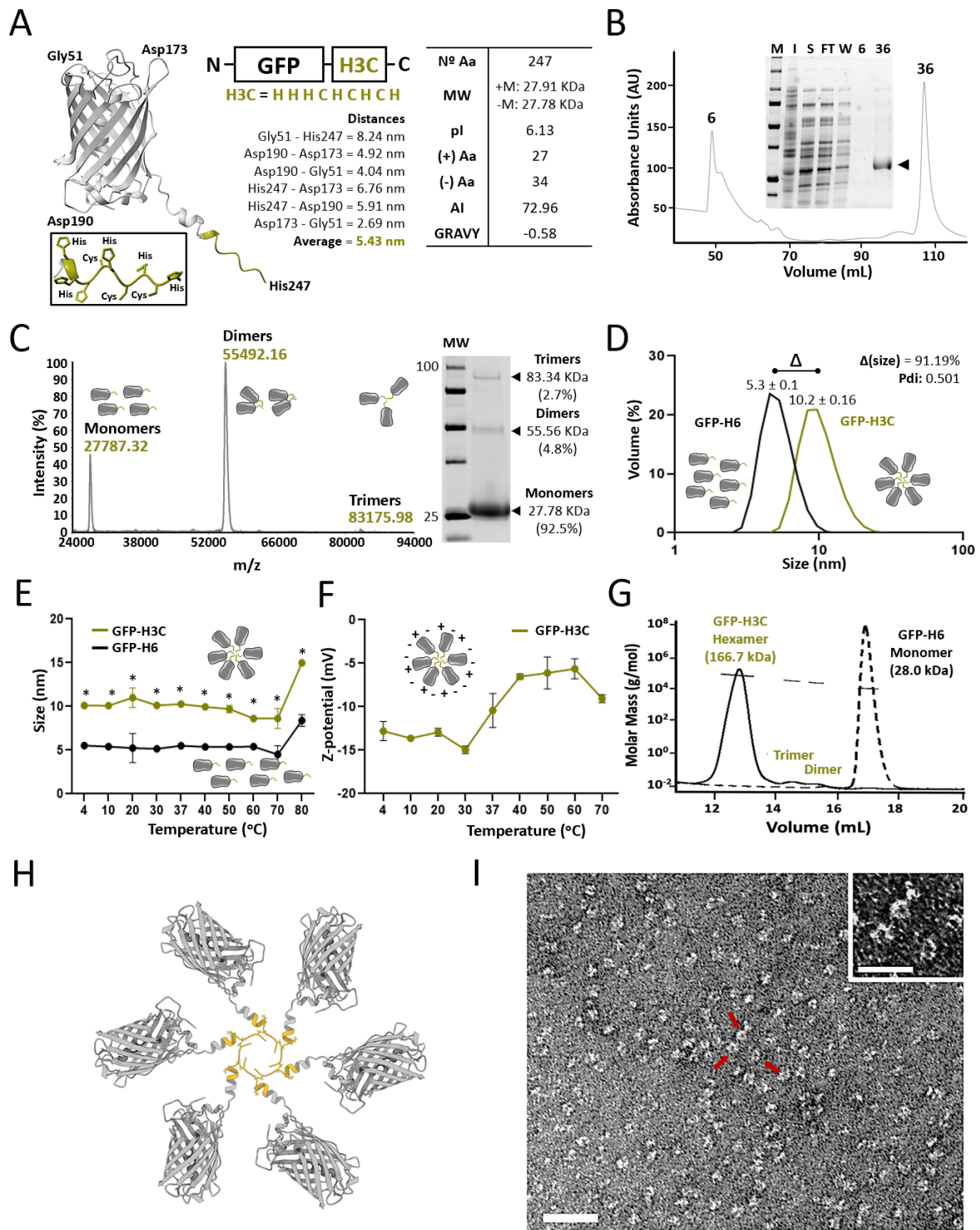


Figure 1. Physicochemical characterization and architecture of GFP-H3C nanoparticles. **A.** Modular protein design and *in silico* 3D structure prediction of GFP-H3C (H3C structure with its respective amino acid side chains is depicted in the inset). H3C tag is displayed in dark yellow and distances between most external amino acids within the structure are measured in order to estimate the average size of the monomer. On the right, a table showing the main physicochemical parameters of GFP-H3C. MW: Molecular weight in presence (+M) or absence

(-M) of the N-terminal methionine. Ip: Isoelectric Point, (+) or (-) Aa: number of positively or negatively charged Amino acids in the primary sequence at physiological pH, AI: Aliphatic Index, GRAVY: Grand average of hydropathicity index **B.** IMAC profile of GFP-H3C protein eluted in a one-step process. The SDS-PAGE gel (inset) shows protein purity in each purification step or sample fraction. M: molecular weight marker, I: insoluble fraction, S: charged soluble cell fraction, FT: flow through, W: wash. 6 and 36 refer to chromatogram protein peaks. **C.** MALDI-TOF spectrum of GFP-H3C protein (24000-94000 Da range). Peak numbers indicate molecular weights in Da. On the right, SDS-PAGE gel showing multimeric forms of GFP-H3C protein. Molecular weight marker (MW) is indicated in kDa and the percentage of each protein subpopulation is shown. **D.** Volume size distribution of purified GFP-H3C (dark yellow) and control GFP-H6 (black) assessed by DLS. Peak values refer to size (in nm) \pm SE. Δ refers to the percentage of GFP-H3C size increase in comparison to the control GFP-H6. Pdi (polydispersion index) of GFP-H3C. **E.** Oligomer size (in nm) of GFP-H3C (dark yellow) and control GFP-H6 (black) at increasing temperatures (from 4 to 80 °C). Significant differences between GFP-H6 and GFP-H3C are indicated (*) at $p < 0.05$. **F.** Zeta-potential (in mV) of GFP-H3C at increasing temperatures (from 4 to 70 °C). Displayed cartoons in the different panels illustrate the oligomerization state of the protein. **G.** Average molar mass (in kDa) of GFP-H6 control monomers (solid line) and GFP-H3C nanoparticles (dashed line) determined by SEC-MALS. **H.** *In silico* representation of cysteine interactions supporting a GFP-H3C nanoparticle. **I.** Morphometric analysis of GFP-H3C nanoparticles by transmission electron microscopy (TEM). White bar indicates 50 nm (25nm in the inset).

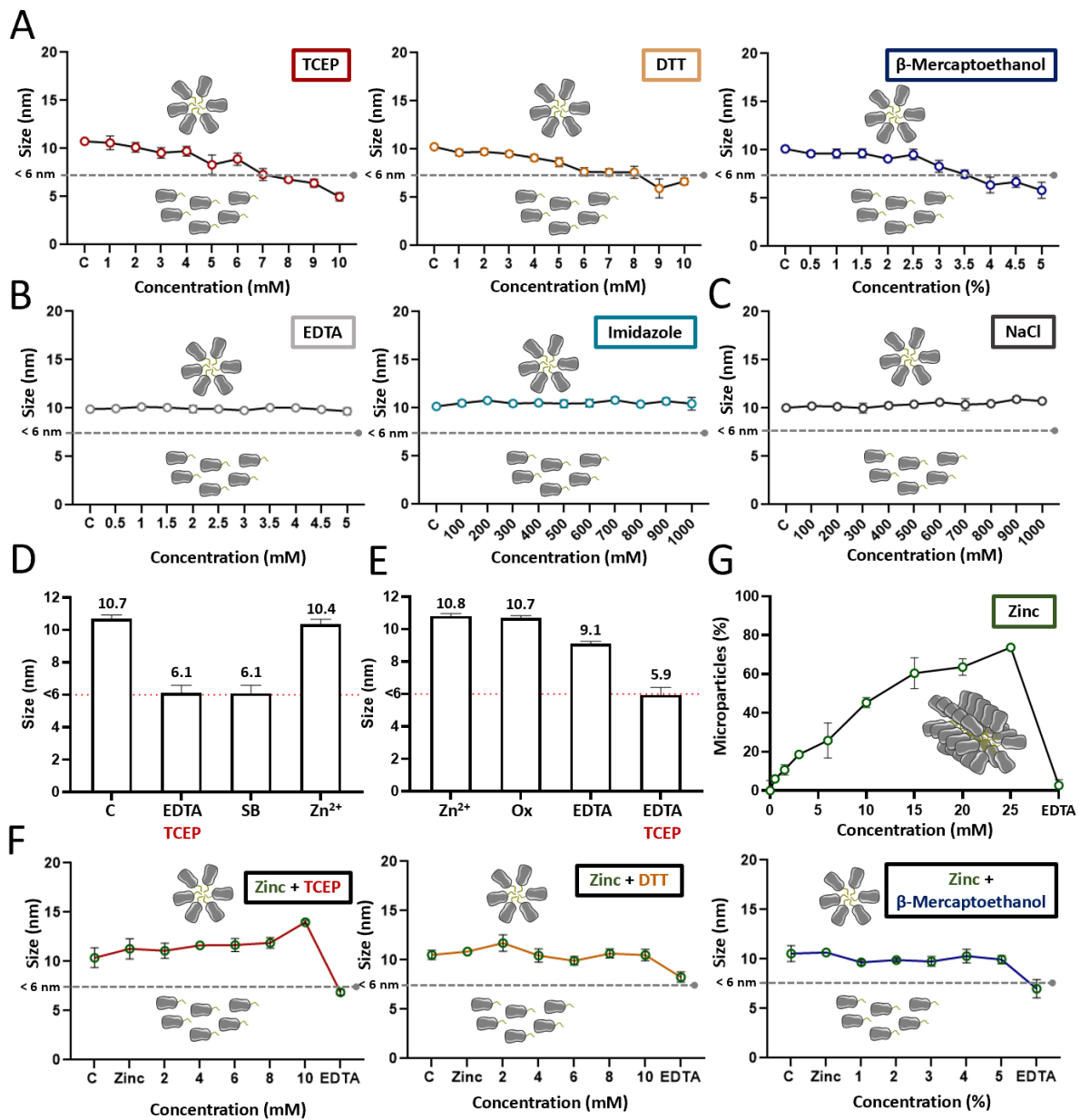


Figure 2. Analysis of protein-protein interactions within supramolecular complexes and microparticles formation. **A.** GFP-H3C nanoparticles incubation at increasing concentrations of different reducing agents (TCEP, DTT and β -Mercaptoethanol). **B.** GFP-H3 nanoparticles incubation at increasing concentrations of cation-arresting molecules (Imidazole, EDTA). **C.** GFP-H3 nanoparticles incubation at increasing concentrations of NaCl. **D.** Cation-promoted assembly of GFP-H3C monomers. Control GFP-H3C nanoparticles (C) are first disassembled (EDTA + TCEP) and then dialyzed against Sodium Bicarbonate solution (SB), or Sodium Bicarbonate solution with 0.4 mM of cationic zinc (Zn^{2+}). **E.** Reducing agent dependent nanoparticle disassembling. Alkaline pH-induced re-oxidation of cysteines (Ox), in previous cation promoted GFP-H3C nanoparticles (Zn^{2+}), are disassembled in presence of a disulfide

reducing agent (EDTA + TCEP) but not upon mere cation arresting (EDTA). **F.** GFP-H3C nanoparticles supplemented with external cations at 0.5 mM (zinc) and incubation at increasing concentrations of reducing agents (Zinc + TCEP), (Zinc + DTT) and (Zinc + β -Mercaptoethanol). EDTA: refers to the final addition of Ethylenediaminetetraacetic acid at 5 mM. **G.** GFP-H3C microparticles formation at increasing concentrations of zinc cations. EDTA: refers to the final addition of Ethylenediaminetetraacetic acid at 10 mM. C always refers to control GFP-H3C nanoparticles. Samples below 6 nm are considered as building blocks (Unassembled protein conformer). Each reagent employed is depicted with a unique color.

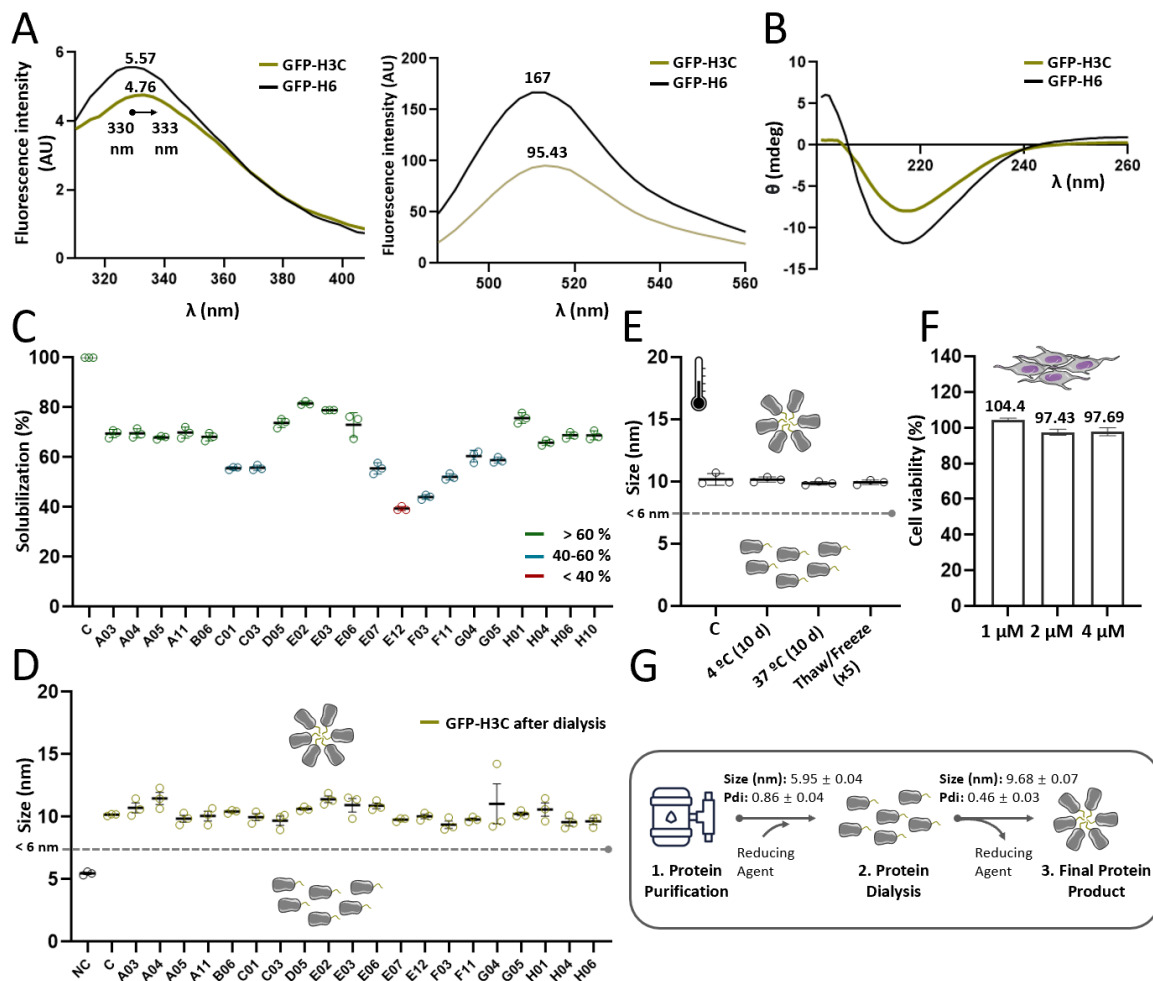


Figure 3. Arrangement stability and toxicity of the GFP-H3C protein material. **A.** Fluorescence emission spectra of protein tryptophan (left panel) recorded between 310 and 560 nm in GFP-H3C (dark yellow) and control GFP-H6 (black) upon excitation at 295 nm. An efficient intramolecular energy transfer from Trp to the GFP chromophore can be observed (right panel). Peak values refer to the fluorescence intensity in arbitrary units (AU). **B.** Circular dichroism (CD) analysis of GFP-H3C (dark yellow) and control GFP-H6 (black) displayed as ellipticity (in mdeg). **C.** GFP-H3C protein solubility (expressed in percentage) screened in a wide range of FDA-approved solutions (see solutions' composition in table S1). C refers to GFP-H3C nanoparticles solubility control in the storage sodium bicarbonate storage solution. **D.** GFP-H3C nanoparticle size (in nm) assessed by DLS in screened FDA-approved solutions. NC refers to a control of negative assembling (GFP-H6 - black) and C refers to control of a GFP-H3C nanoparticle assembling in sodium bicarbonate storage solution. Samples below 6 nm are considered as building blocks. **E.** Size stability (in nm) assessed by DLS upon protein incubation at 4 and 37 °C for 10 days, and after 5 cycles of thawing and freezing. Samples

below 6 nm are considered as building blocks. **F.** HeLa cells viability assay (expressed in percentage) upon incubation at increasing concentrations of GFP-H3C nanoparticles (1, 2 and 4 μM) for 48 h. **G.** A schematic representation of the protein oligomeric state during the formulation procedure. Size values (in nm), as well as Pdi are displayed as mean size \pm SE (Standard error).

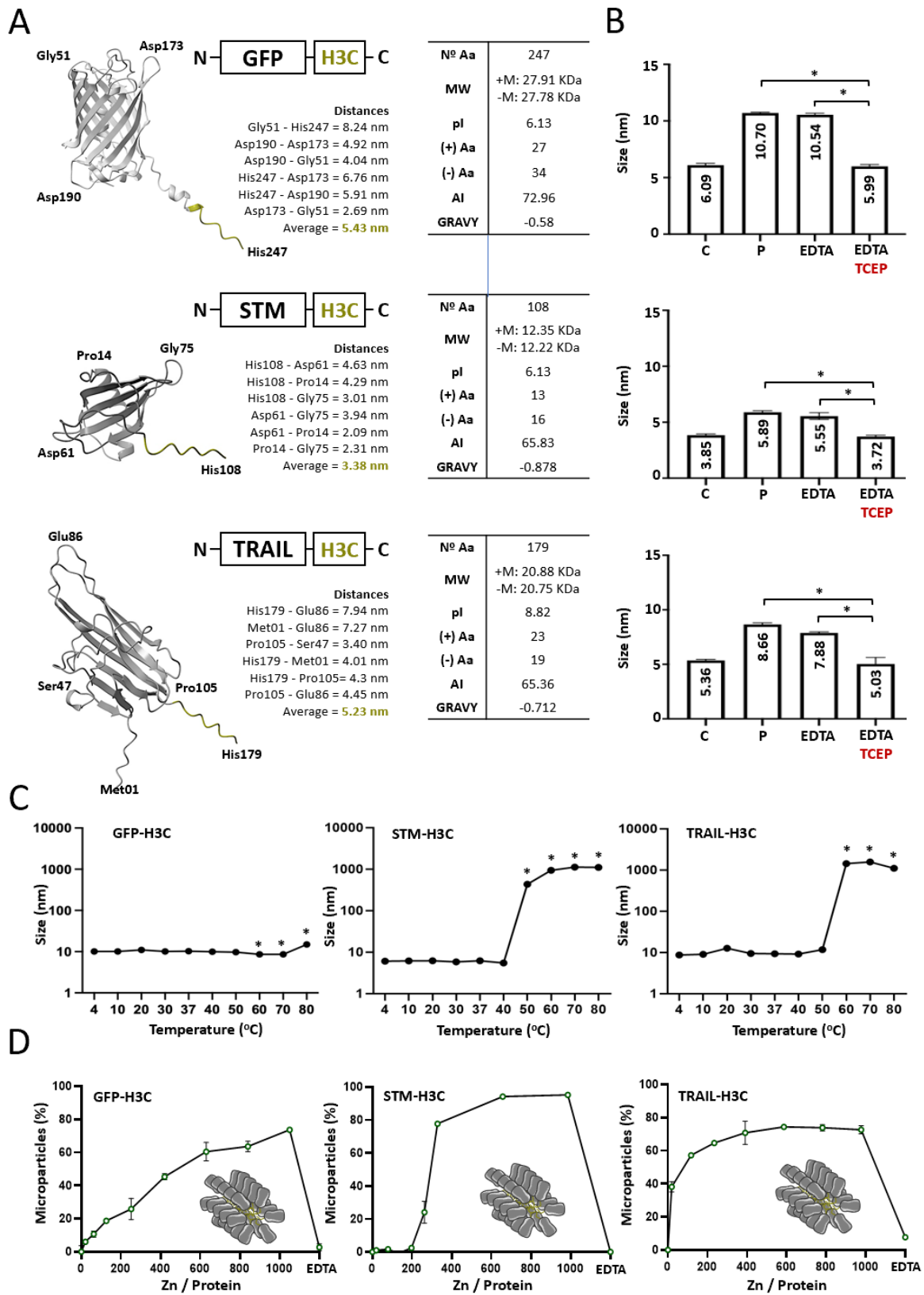


Figure 4. Physicochemical characterization and formulation of GFP-H3C, STM-H3C and TRAIL-H3C nanoparticles **A.** Modular protein design and *in-silico* 3D structure prediction of

GFP-H3, STM-H3C and TRAIL-H3C proteins. H3C tags are displayed in dark yellow and distances between most external amino acids within the protein structures are measured in order to estimate their average monomer size. On the right, a table showing the main physicochemical parameters of each protein. MW: Molecular weight in presence (+M) or absence (-M) of the N-terminal methionine, pI: Theoretical isoelectric point, (+) or (-) Aa: number of positively or negatively charged amino acids in the primary sequence at physiological pH, AI: Aliphatic Index, GRAVY: Grand average of hydropathicity index. **B.** Volume size distribution of purified protein nanoparticles assessed by DLS. C refers to SDS-disassembled protein building blocks. P refers to purified protein nanoparticles. EDTA refers to the addition of Ethylenediaminetetraacetic acid at 5 mM concentration. TCEP (depicted in red) refers to the addition of the reducing agent TCEP at 2mM for STM-H3C, 5 mM for TRAIL-H3C and 10 mM for GFP-H3C. Peak values refer to average size \pm SE **C.** GFP-H3C, STM-H3C and TRAIL-H3C nanoparticles size at increasing temperatures (from 4 to 80 °C). Significant differences between 4 °C and the rest of temperatures are indicated as (*) when $p < 0.05$. **D.** GFP-H3C, STM-H3C and TRAIL-H3C microparticles formation at increasing concentrations of zinc cations expressed as zinc / protein molar ratio. EDTA: refers to the final addition of Ethylenediaminetetraacetic acid at 10 mM.

SUPPORTING INFORMATION

Supplementary figure with amino acid sequence of GFP-H3C, STM-H3C and TRAIL-H3C proteins. Supplementary figure with MALDI-TOF spectrum of purified STM-H3C and TRAIL-H3C proteins. Supplementary figure with SDS-PAGE and Western-blot immunodetection of STM-H3C and TRAIL-H3C proteins. Supplementary figure with microscopy images showing multistage transition of GFP-H3C, STM-H3C and TRAIL-H3C nanoparticles to cation-induced microparticles. Supplementary table with Nomenclature and Composition FDA-approved solutions.

ACKNOWLEDGEMENTS

Hector Lopez-Laguna and Ariana Rueda contributed equally to this work. The authors are indebted to Agencia Estatal de Investigación (PID2020-116174RB-I00) granted to AV; to ISCIII (PI20/00400) co-funded by European Regional Development Fund (ERDF, a way to make Europe) and to CIBER-BBN (project NANOSCAPE and NANOLINK) granted to UU; to AEI (PID2019-105416RB-I00/AEI/10.13039/501100011033), and to CIBER-BBN (NANOREMOTE) granted to EV, to AEI (PID2019-107298RB-C22) granted to NFM, to Ministerio de Ciencia, Innovación y Universidades (PGC2018-098423-B-I00) granted to DR and to ISCIII (PI21/00150) co-funded by European Regional Development Fund (ERDF, a way to make Europe), to CIBER-BBN (4NanoMets) and to AGAUR (2017 SGR-865) granted to RM. This research was also supported by CIBER -Consortio Centro de Investigación Biomédica en Red- (CB06/01/1031 and CB06/01/0014), Instituto de Salud Carlos III, Ministerio de Ciencia e Innovación and European Regional Development Fund (ERDF) and by CERCA programme (Generalitat de Catalunya). UU is supported by Miguel Servet contract (CP19/00028) from ISCIII co-funded by European Social Fund (ESF investing in your future). HLL. received a predoctoral fellowship from AGAUR (2019 FI_B 00352). AR was supported by a PFIS predoctoral fellowship (FI21/00012) from ISCIII co-funded by European Social Fund (ESF, investing in your future). LSA was supported by a predoctoral fellowship from the Ministerio de Ciencia, Innovación y Universidades (FPI18/04615). EVD was supported by a predoctoral fellowship from the Ministerio de Ciencia, Innovación y Universidades (FPU18/04615). JAG was supported by a predoctoral fellowship from Ministerio de Universidades (FPU20/02260). AV received an Icrea Academia award. Protein production was partially performed by the ICTS “NANBIOSIS”, more specifically by the Protein Production Platform of CIBER in Bioengineering, Biomaterials & Nanomedicine (CIBER-BBN)/ IBB, at the UAB <http://www.nanbiosis.es/portfolio/u1-protein-production-platform-ppp/>. Molecular

graphics were performed with UCSF ChimeraX, developed by the Resource for Biocomputing, Visualization, and Informatics at the University of California, San Francisco, with support from National Institutes of Health R01-GM129325 and the Office of Cyber Infrastructure and Computational Biology, National Institute of Allergy and Infectious Diseases.

AUTHOR INFORMATION

Corresponding Author

Ugutx Unzueta: UUnzueta@santpau.cat

Esther Vazquez: esther.vazquez@uab.es

Antonio Villaverde: antoni.villaverde@uab.cat

Conflict of Interest:

Authors declare no conflict of interest.

Author Contributions

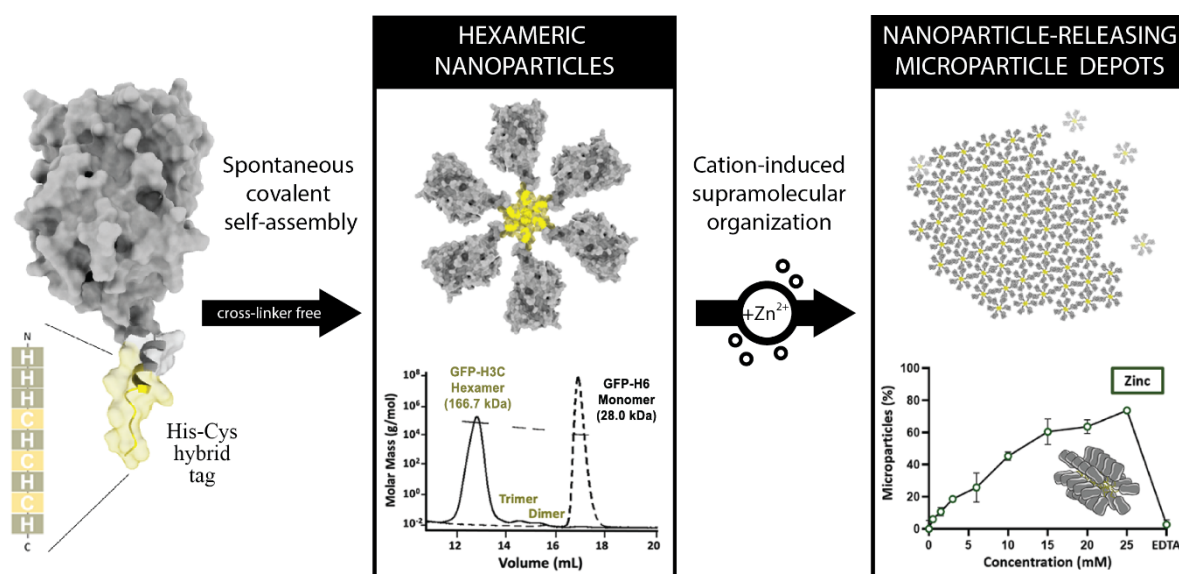
The manuscript was written through contributions of all authors. All authors have given approval to the final version of the manuscript. ‡These authors contributed equally.

Present Addresses

† Nanoligent, S.L. Edifici Eureka, Campus de la UAB, 08193 Bellaterra, Spain.

TABLE OF CONTENTS:

This work reports the rational engineering of an innovative architectonic peptide tag (H3C) that by strategically combining cysteine and histidine residues within the sequence, allows the spontaneous and cross-linker free self-assembling of proteins into a covalent nanoparticle through a histidine-templated cysteine coupling process. This hybrid tag allows also the histidine-mediated and zinc-induced supramolecular organization of nanoparticles into higher-order microparticulate materials as nanoparticle-releasing depots.



REFERENCES:

- (1) Wang, S.-T.; Minevich, B.; Liu, J.; Zhang, H.; Nykypanchuk, D.; Byrnes, J.; Liu, W.; Bershadsky, L.; Liu, Q.; Wang, T.; Ren, G.; Gang, O. Designed and Biologically Active Protein Lattices. *Nat Commun* **2021**, *12* (1), 3702. <https://doi.org/10.1038/s41467-021-23966-4>.
- (2) Tang, T.-C.; An, B.; Huang, Y.; Vasikaran, S.; Wang, Y.; Jiang, X.; Lu, T. K.; Zhong, C. Materials Design by Synthetic Biology. *Nat Rev Mater* **2021**, *6* (4), 332–350. <https://doi.org/10.1038/s41578-020-00265-w>.
- (3) Mendes, A. C.; Baran, E. T.; Reis, R. L.; Azevedo, H. S. Self-Assembly in Nature: Using the Principles of Nature to Create Complex Nanobiomaterials. *Wiley Interdiscip Rev Nanomed Nanobiotechnol* **2013**, *5* (6), 582–612. <https://doi.org/10.1002/wnan.1238>.
- (4) Howorka, S. Rationally Engineering Natural Protein Assemblies in Nanobiotechnology. *Curr Opin Biotechnol* **2011**, *22* (4), 485–491. <https://doi.org/10.1016/j.copbio.2011.05.003>.
- (5) Korpi, A.; Anaya-Plaza, E.; Välimäki, S.; Kostianen, M. Highly Ordered Protein Cage Assemblies: A Toolkit for New Materials. *WIREs Nanomedicine and Nanobiotechnology* **2020**, *12* (1). <https://doi.org/10.1002/wnan.1578>.
- (6) Ulijn, R. v.; Lampel, A. Order/Disorder in Protein and Peptide-Based Biomaterials. *Isr J Chem* **2020**, *60* (12), 1129–1140. <https://doi.org/10.1002/ijch.201900051>.
- (7) Hansen, W. A.; Khare, S. D. Recent Progress in Designing Protein-Based Supramolecular Assemblies. *Curr Opin Struct Biol* **2020**, *63*, 106–114. <https://doi.org/10.1016/j.sbi.2020.05.001>.
- (8) Hamley, I. W. Protein Assemblies: Nature-Inspired and Designed Nanostructures. *Biomacromolecules* **2019**, *20* (5), 1829–1848. <https://doi.org/10.1021/acs.biomac.9b00228>.
- (9) Li, J.; Li, S.; Huang, J.; Khan, A. Q.; An, B.; Zhou, X.; Liu, Z.; Zhu, M. Spider Silk-Inspired Artificial Fibers. *Advanced Science* **2022**, *9* (5), 2103965. <https://doi.org/10.1002/advs.202103965>.
- (10) Du, P.; Xu, S.; Xu, Z.; Wang, Z. Bioinspired Self-Assembling Materials for Modulating Enzyme Functions. *Adv Funct Mater* **2021**, *31* (38), 2104819. <https://doi.org/10.1002/adfm.202104819>.
- (11) Delfi, M.; Sartorius, R.; Ashrafizadeh, M.; Sharifi, E.; Zhang, Y.; de Berardinis, P.; Zarrabi, A.; Varma, R. S.; Tay, F. R.; Smith, B. R.; Makvandi, P. Self-Assembled Peptide and Protein Nanostructures for Anti-Cancer Therapy: Targeted Delivery, Stimuli-Responsive Devices and Immunotherapy. *Nano Today* **2021**, *38*, 101119. <https://doi.org/10.1016/j.nantod.2021.101119>.
- (12) Sarangthem, V.; Singh, T. D.; Dinda, A. K. Emerging Role of Elastin-Like Polypeptides in Regenerative Medicine. *Adv Wound Care (New Rochelle)* **2021**, *10* (5), 257–269. <https://doi.org/10.1089/wound.2019.1085>.
- (13) Muzzio, N.; Moya, S.; Romero, G. Multifunctional Scaffolds and Synergistic Strategies in Tissue Engineering and Regenerative Medicine. *Pharmaceutics* **2021**, *13* (6), 792. <https://doi.org/10.3390/pharmaceutics13060792>.
- (14) Gopalakrishnan, S.; Xu, J.; Zhong, F.; Rotello, V. M. Strategies for Fabricating Protein Films for Biomaterial Applications. *Adv Sustain Syst* **2021**, *5* (1), 2000167. <https://doi.org/10.1002/adsu.202000167>.
- (15) Shim, J.; Zhou, C.; Gong, T.; Iserlis, D. A.; Linjawati, H. A.; Wong, M.; Pan, T.; Tan, C. Building Protein Networks in Synthetic Systems from the Bottom-Up. *Biotechnol Adv* **2021**, *49*, 107753. <https://doi.org/10.1016/j.biotechadv.2021.107753>.

- (16) Wichgers Schreur, P. J.; Tacke, M.; Gutjahr, B.; Keller, M.; van Keulen, L.; Kant, J.; van de Water, S.; Lin, Y.; Eiden, M.; Rissmann, M.; von Arnim, F.; König, R.; Brix, A.; Charreyre, C.; Audonnet, J.-C.; Groschup, M. H.; Kortekaas, J. Vaccine Efficacy of Self-Assembled Multimeric Protein Scaffold Particles Displaying the Glycoprotein Gn Head Domain of Rift Valley Fever Virus. *Vaccines (Basel)* **2021**, *9* (3), 301. <https://doi.org/10.3390/vaccines9030301>.
- (17) Vulovic, I.; Yao, Q.; Park, Y.-J.; Courbet, A.; Norris, A.; Busch, F.; Sahasrabudhe, A.; Merten, H.; Sahtoe, D. D.; Ueda, G.; Fallas, J. A.; Weaver, S. J.; Hsia, Y.; Langan, R. A.; Plückthun, A.; Wysocki, V. H.; Veessler, D.; Jensen, G. J.; Baker, D. Generation of Ordered Protein Assemblies Using Rigid Three-Body Fusion. *Proceedings of the National Academy of Sciences* **2021**, *118* (23). <https://doi.org/10.1073/pnas.2015037118>.
- (18) Unzueta, U.; Ferrer-Miralles, N.; Cedano, J.; Zikung, X.; Pesarrodona, M.; Saccardo, P.; García-Fruitós, E.; Domingo-Espín, J.; Kumar, P.; Gupta, K. C.; Mangués, R.; Villaverde, A.; Vázquez, E. Non-Amyloidogenic Peptide Tags for the Regulatable Self-Assembling of Protein-Only Nanoparticles. *Biomaterials* **2012**, *33* (33), 8714–8722. <https://doi.org/10.1016/j.biomaterials.2012.08.033>.
- (19) Hassanin, I. A.; Elzoghby, A. O. Self-Assembled Non-Covalent Protein-Drug Nanoparticles: An Emerging Delivery Platform for Anti-Cancer Drugs. *Expert Opin Drug Deliv* **2020**, *17* (10), 1437–1458. <https://doi.org/10.1080/17425247.2020.1813713>.
- (20) Volodkin, D. v.; Schmidt, S.; Fernandes, P.; Larionova, N. I.; Sukhorukov, G. B.; Duschl, C.; Möhwald, H.; von Klitzing, R. One-Step Formulation of Protein Microparticles with Tailored Properties: Hard Templating at Soft Conditions. *Adv Funct Mater* **2012**, *22* (9), 1914–1922. <https://doi.org/10.1002/adfm.201103007>.
- (21) Zhou, K.; Chen, H.; Zhang, S.; Wang, Y.; Zhao, G. Disulfide-Mediated Reversible Two-Dimensional Self-Assembly of Protein Nanocages. *Chemical Communications* **2019**, *55* (52), 7510–7513. <https://doi.org/10.1039/C9CC03085A>.
- (22) Mak, W. C.; Georgieva, R.; Renneberg, R.; Bäumler, H. Protein Particles Formed by Protein Activation and Spontaneous Self-Assembly. *Adv Funct Mater* **2010**, *20* (23), 4139–4144. <https://doi.org/10.1002/adfm.201001205>.
- (23) López-Laguna, H.; Sánchez, J. M.; Carratalá, J. V.; Rojas-Peña, M.; Sánchez-García, L.; Parladé, E.; Sánchez-Chardi, A.; Voltà-Durán, E.; Serna, N.; Cano-Garrido, O.; Flores, S.; Ferrer-Miralles, N.; Nolan, V.; de Marco, A.; Roher, N.; Unzueta, U.; Vázquez, E.; Villaverde, A. Biofabrication of Functional Protein Nanoparticles through Simple His-Tag Engineering. *ACS Sustain Chem Eng* **2021**, *9* (36), 12341–12354. <https://doi.org/10.1021/acssuschemeng.1c04256>.
- (24) López-Laguna, H.; Voltà-Durán, E.; Parladé, E.; Villaverde, A.; Vázquez, E.; Unzueta, U. Insights on the Emerging Biotechnology of Histidine-Rich Peptides. *Biotechnol Adv* **2022**, *54*, 107817. <https://doi.org/10.1016/j.biotechadv.2021.107817>.
- (25) Pina, A. S.; Batalha, Í. L.; Dias, A. M. G. C.; Roque, A. C. A. Affinity Tags in Protein Purification and Peptide Enrichment: An Overview; 2021; pp 107–132. https://doi.org/10.1007/978-1-0716-0775-6_10.
- (26) López-Laguna, H.; Sánchez, J.; Unzueta, U.; Mangués, R.; Vázquez, E.; Villaverde, A. Divalent Cations: A Molecular Glue for Protein Materials. *Trends Biochem Sci* **2020**, *45* (11), 992–1003. <https://doi.org/10.1016/j.tibs.2020.08.003>.
- (27) López-Laguna, H.; Sánchez-García, L.; Serna, N.; Voltà-Durán, E.; Sánchez, J. M.; Sánchez-Chardi, A.; Unzueta, U.; Łoś, M.; Villaverde, A.; Vázquez, E. Engineering Protein Nanoparticles Out from Components of the Human Microbiome. *Small* **2020**, *16* (30), 2001885. <https://doi.org/10.1002/sml.202001885>.

- (28) Chen, T.-Y.; Cheng, W.-J.; Horng, J.-C.; Hsu, H.-Y. Artificial Peptide-Controlled Protein Release of Zn²⁺-Triggered, Self-Assembled Histidine-Tagged Protein Microparticle. *Colloids Surf B Biointerfaces* **2020**, *187*, 110644. <https://doi.org/10.1016/j.colsurfb.2019.110644>.
- (29) Knight, A. S.; Larsson, J.; Ren, J. M.; Bou Zerdan, R.; Seguin, S.; Vrahas, R.; Liu, J.; Ren, G.; Hawker, C. J. Control of Amphiphile Self-Assembly via Bioinspired Metal Ion Coordination. *J Am Chem Soc* **2018**, *140* (4), 1409–1414. <https://doi.org/10.1021/jacs.7b11005>.
- (30) Jehle, F.; Fratzl, P.; Harrington, M. J. Metal-Tunable Self-Assembly of Hierarchical Structure in Mussel-Inspired Peptide Films. *ACS Nano* **2018**, *12* (3), 2160–2168. <https://doi.org/10.1021/acsnano.7b07905>.
- (31) Falgàs, A.; Pallarès, V.; Unzueta, U.; Núñez, Y.; Sierra, J.; Gallardo, A.; Alba-Castellón, L.; Mangués, M. A.; Álamo, P.; Villaverde, A.; Vázquez, E.; Mangués, R.; Casanova, I. Specific Cytotoxic Effect of an Auristatin Nanoconjugate Towards CXCR4+ Diffuse Large B-Cell Lymphoma Cells. *Int J Nanomedicine* **2021**, *Volume 16*, 1869–1888. <https://doi.org/10.2147/IJN.S289733>.
- (32) Pallarès, V.; Unzueta, U.; Falgàs, A.; Aviñó, A.; Núñez, Y.; García-León, A.; Sánchez-García, L.; Serna, N.; Gallardo, A.; Alba-Castellón, L.; Álamo, P.; Sierra, J.; Cedó, L.; Eritja, R.; Villaverde, A.; Vázquez, E.; Casanova, I.; Mangués, R. A Multivalent Ara-C-Prodrug Nanoconjugate Achieves Selective Ablation of Leukemic Cells in an Acute Myeloid Leukemia Mouse Model. *Biomaterials* **2022**, *280*, 121258. <https://doi.org/10.1016/j.biomaterials.2021.121258>.
- (33) Céspedes, M. V.; Unzueta, U.; Aviñó, A.; Gallardo, A.; Álamo, P.; Sala, R.; Sánchez-Chardi, A.; Casanova, I.; Mangués, M. A.; Lopez-Pousa, A.; Eritja, R.; Villaverde, A.; Vázquez, E.; Mangués, R. Selective Depletion of Metastatic Stem Cells as Therapy for Human Colorectal Cancer. *EMBO Mol Med* **2018**, *10* (10). <https://doi.org/10.15252/emmm.201708772>.
- (34) Rioja-Blanco, E.; Arroyo-Solera, I.; Álamo, P.; Casanova, I.; Gallardo, A.; Unzueta, U.; Serna, N.; Sánchez-García, L.; Quer, M.; Villaverde, A.; Vázquez, E.; Mangués, R.; Alba-Castellón, L.; León, X. Self-Assembling Protein Nanocarrier for Selective Delivery of Cytotoxic Polypeptides to CXCR4+ Head and Neck Squamous Cell Carcinoma Tumors. *Acta Pharm Sin B* **2022**, *12* (5), 2578–2591. <https://doi.org/10.1016/j.apsb.2021.09.030>.
- (35) Sánchez-García, L.; Voltà-Durán, E.; Parladé, E.; Mazzega, E.; Sánchez-Chardi, A.; Serna, N.; López-Laguna, H.; Mitstorfer, M.; Unzueta, U.; Vázquez, E.; Villaverde, A.; de Marco, A. Self-Assembled Nanobodies as Selectively Targeted, Nanostructured, and Multivalent Materials. *ACS Appl Mater Interfaces* **2021**, *13* (25), 29406–29415. <https://doi.org/10.1021/acsmi.1c08092>.
- (36) Cano-Garrido, O.; Álamo, P.; Sánchez-García, L.; Falgàs, A.; Sánchez-Chardi, A.; Serna, N.; Parladé, E.; Unzueta, U.; Roldán, M.; Voltà-Durán, E.; Casanova, I.; Villaverde, A.; Mangués, R.; Vázquez, E. Biparatopic Protein Nanoparticles for the Precision Therapy of CXCR4+ Cancers. *Cancers (Basel)* **2021**, *13* (12), 2929. <https://doi.org/10.3390/cancers13122929>.
- (37) Serna, N.; Carratalá, J. V.; Conchillo-Solé, O.; Martínez-Torró, C.; Unzueta, U.; Mangués, R.; Ferrer-Miralles, N.; Daura, X.; Vázquez, E.; Villaverde, A. Antibacterial Activity of T22, a Specific Peptidic Ligand of the Tumoral Marker CXCR4. *Pharmaceutics* **2021**, *13* (11), 1922. <https://doi.org/10.3390/pharmaceutics13111922>.
- (38) Voltà-Durán, E.; Sánchez, J. M.; López-Laguna, H.; Parladé, E.; Sánchez-García, L.; Sánchez-Chardi, A.; de Marco, A.; Unzueta, U.; Vázquez, E.; Villaverde, A. The Spectrum of Building Block Conformers Sustains the Biophysical Properties of

- Clinically-Oriented Self-Assembling Protein Nanoparticles. *Sci China Mater* **2022**, *65* (6), 1662–1670. <https://doi.org/10.1007/s40843-021-1914-0>.
- (39) Jumper, J.; Evans, R.; Pritzel, A.; Green, T.; Figurnov, M.; Ronneberger, O.; Tunyasuvunakool, K.; Bates, R.; Žídek, A.; Potapenko, A.; Bridgland, A.; Meyer, C.; Kohl, S. A. A.; Ballard, A. J.; Cowie, A.; Romera-Paredes, B.; Nikolov, S.; Jain, R.; Adler, J.; Back, T.; Petersen, S.; Reiman, D.; Clancy, E.; Zielinski, M.; Steinegger, M.; Pacholska, M.; Berghammer, T.; Bodenstein, S.; Silver, D.; Vinyals, O.; Senior, A. W.; Kavukcuoglu, K.; Kohli, P.; Hassabis, D. Highly Accurate Protein Structure Prediction with AlphaFold. *Nature* **2021**, *596* (7873), 583–589. <https://doi.org/10.1038/s41586-021-03819-2>.
- (40) Mirdita, M.; Schütze, K.; Moriwaki, Y.; Heo, L.; Ovchinnikov, S.; Steinegger, M. ColabFold: Making Protein Folding Accessible to All. *Nat Methods* **2022**, *19* (6), 679–682. <https://doi.org/10.1038/s41592-022-01488-1>.
- (41) Wilkins, M. R.; Gasteiger, E.; Bairoch, A.; Sanchez, J.-C.; Williams, K. L.; Appel, R. D.; Hochstrasser, D. F. Protein Identification and Analysis Tools in the ExPASy Server. In *2-D Proteome Analysis Protocols*; Humana Press: New Jersey; pp 531–552. <https://doi.org/10.1385/1-59259-584-7:531>.
- (42) Sánchez, J. M.; Sánchez-García, L.; Pesarrodonna, M.; Serna, N.; Sánchez-Chardi, A.; Unzueta, U.; Mangues, R.; Vázquez, E.; Villaverde, A. Conformational Conversion during Controlled Oligomerization into Nonamylogenic Protein Nanoparticles. *Biomacromolecules* **2018**, *19* (9), 3788–3797. <https://doi.org/10.1021/acs.biomac.8b00924>.
- (43) Rigüero, V.; Clifford, R.; Dawley, M.; Dickson, M.; Gastfriend, B.; Thompson, C.; Wang, S.-C.; O'Connor, E. Immobilized Metal Affinity Chromatography Optimization for Poly-Histidine Tagged Proteins. *J Chromatogr A* **2020**, *1629*, 461505. <https://doi.org/10.1016/j.chroma.2020.461505>.
- (44) Yang, Y.; Mitri, K.; Zhang, C.; Boysen, R. I.; Hearn, M. T. W. Promiscuity of Host Cell Proteins in the Purification of Histidine Tagged Recombinant Xylanase A by IMAC Procedures: A Case Study with a Ni²⁺-Tacn-Based IMAC System. *Protein Expr Purif* **2019**, *162*, 51–61. <https://doi.org/10.1016/j.pep.2019.05.009>.
- (45) Loughran, S. T.; Bree, R. T.; Walls, D. Purification of Polyhistidine-Tagged Proteins; 2017; pp 275–303. https://doi.org/10.1007/978-1-4939-6412-3_14.
- (46) Zhang, J.; Wang, X.; Zhou, K.; Chen, G.; Wang, Q. Self-Assembly of Protein Crystals with Different Crystal Structures Using Tobacco Mosaic Virus Coat Protein as a Building Block. *ACS Nano* **2018**, *12* (2), 1673–1679. <https://doi.org/10.1021/acs.nano.7b08316>.
- (47) Knecht, S.; Ricklin, D.; Eberle, A. N.; Ernst, B. Oligohis-Tags: Mechanisms of Binding to Ni²⁺-NTA Surfaces. *Journal of Molecular Recognition* **2009**, *22* (4), 270–279. <https://doi.org/10.1002/jmr.941>.
- (48) Liu, Z.; Behloul, N.; Baha, S.; Wei, W.; Tao, W.; Zhang, T.; Li, W.; Shi, R.; Meng, J. Role of the C-Terminal Cysteines in Virus-like Particle Formation and Oligomerization of the Hepatitis E Virus ORF2 Truncated Proteins. *Virology* **2020**, *544*, 1–11. <https://doi.org/10.1016/j.virol.2020.01.011>.
- (49) JAIN, R. K.; JOYCE, P. B. M.; MOLINETE, M.; HALBAN, P. A.; GORR, S.-U. Oligomerization of Green Fluorescent Protein in the Secretory Pathway of Endocrine Cells. *Biochemical Journal* **2001**, *360* (3), 645. <https://doi.org/10.1042/0264-6021:3600645>.
- (50) Suzuki, T.; Arai, S.; Takeuchi, M.; Sakurai, C.; Ebana, H.; Higashi, T.; Hashimoto, H.; Hatsuzawa, K.; Wada, I. Development of Cysteine-Free Fluorescent Proteins for the Oxidative Environment. *PLoS One* **2012**, *7* (5), e37551. <https://doi.org/10.1371/journal.pone.0037551>.

- (51) Wingfield, P. T. N-Terminal Methionine Processing. *Curr Protoc Protein Sci* **2017**, 88 (1). <https://doi.org/10.1002/cpps.29>.
- (52) Sánchez, J. M.; López-Laguna, H.; Álamo, P.; Serna, N.; Sánchez-Chardi, A.; Nolan, V.; Cano-Garrido, O.; Casanova, I.; Unzueta, U.; Vazquez, E.; Mangués, R.; Villaverde, A. Artificial Inclusion Bodies for Clinical Development. *Advanced Science* **2020**, 7 (3), 1902420. <https://doi.org/10.1002/advs.201902420>.
- (53) Céspedes, M. V.; Cano-Garrido, O.; Álamo, P.; Sala, R.; Gallardo, A.; Serna, N.; Falgàs, A.; Voltà-Durán, E.; Casanova, I.; Sánchez-Chardi, A.; López-Laguna, H.; Sánchez-García, L.; Sánchez, J. M.; Unzueta, U.; Vázquez, E.; Mangués, R.; Villaverde, A. Engineering Secretory Amyloids for Remote and Highly Selective Destruction of Metastatic Foci. *Advanced Materials* **2020**, 32 (7), 1907348. <https://doi.org/10.1002/adma.201907348>.
- (54) Sánchez, J. M.; Carratalá, J. V.; Serna, N.; Unzueta, U.; Nolan, V.; Sánchez-Chardi, A.; Voltà-Durán, E.; López-Laguna, H.; Ferrer-Miralles, N.; Villaverde, A.; Vazquez, E. The Poly-Histidine Tag H6 Mediates Structural and Functional Properties of Disintegrating, Protein-Releasing Inclusion Bodies. *Pharmaceutics* **2022**, 14 (3), 602. <https://doi.org/10.3390/pharmaceutics14030602>.
- (55) Jacob, R. S.; Anoop, A.; Maji, S. K. Protein Nanofibrils as Storage Forms of Peptide Drugs and Hormones; 2019; pp 265–290. https://doi.org/10.1007/978-981-13-9791-2_8.
- (56) Jacob, R. S.; Das, S.; Ghosh, S.; Anoop, A.; Jha, N. N.; Khan, T.; Singru, P.; Kumar, A.; Maji, S. K. Amyloid Formation of Growth Hormone in Presence of Zinc: Relevance to Its Storage in Secretory Granules. *Sci Rep* **2016**, 6 (1), 23370. <https://doi.org/10.1038/srep23370>.
- (57) Mankar, S.; Anoop, A.; Sen, S.; Maji, S. K. Nanomaterials: Amyloids Reflect Their Brighter Side. *Nano Rev* **2011**, 2 (1), 6032. <https://doi.org/10.3402/nano.v2i0.6032>.
- (58) Maji, S. K.; Perrin, M. H.; Sawaya, M. R.; Jessberger, S.; Vadodaria, K.; Rissman, R. A.; Singru, P. S.; Nilsson, K. P. R.; Simon, R.; Schubert, D.; Eisenberg, D.; Rivier, J.; Sawchenko, P.; Vale, W.; Riek, R. Functional Amyloids As Natural Storage of Peptide Hormones in Pituitary Secretory Granules. *Science (1979)* **2009**, 325 (5938), 328–332. <https://doi.org/10.1126/science.1173155>.
- (59) Álamo, P.; Parladé, E.; López-Laguna, H.; Voltà-Durán, E.; Unzueta, U.; Vazquez, E.; Mangués, R.; Villaverde, A. Ion-Dependent Slow Protein Release from *in Vivo* Disintegrating Micro-Granules. *Drug Deliv* **2021**, 28 (1), 2383–2391. <https://doi.org/10.1080/10717544.2021.1998249>.
- (60) Hoffmann, T.; Stadler, L. K. J.; Busby, M.; Song, Q.; Buxton, A. T.; Wagner, S. D.; Davis, J. J.; Ko Ferrigno, P. Structure-Function Studies of an Engineered Scaffold Protein Derived from Stefin A. I: Development of the SQM Variant. *Protein Engineering, Design and Selection* **2010**, 23 (5), 403–413. <https://doi.org/10.1093/protein/gzq012>.
- (61) Duiker, E. W.; Mom, C. H.; de Jong, S.; Willemse, P. H. B.; Gietema, J. A.; van der Zee, A. G. J.; de Vries, E. G. E. The Clinical Trail of TRAIL. *Eur J Cancer* **2006**, 42 (14), 2233–2240. <https://doi.org/10.1016/j.ejca.2006.03.018>.